

# Bayesian calibration of a $k - \epsilon$ turbulence model for predictive jet-in-crossflow simulations

Jaideep Ray \* and Sophia Lefantzi †

*Sandia National Laboratories, Livermore, CA 94550-0969, USA*

Srinivasan Arunajatesan ‡ and Lawrence Dechant‡

*Sandia National Laboratories, Albuquerque, NM 87185-5800, USA*

AIAA-2014-2085

We propose a Bayesian method to calibrate parameters of a  $k - \epsilon$  RANS model to improve its predictive skill in jet-in-crossflow simulations. The method is based on the hypotheses that (1) informative parameters can be estimated from experiments of flow configurations that display the same, strongly vortical features of jet-in-crossflow interactions and (2) one can construct surrogates of RANS models for judiciously chosen outputs which serve as calibration observables. We estimate three  $k - \epsilon$  parameters,  $(C_\mu, C_{\epsilon 2}, C_{\epsilon 1})$ , from Reynolds stress measurements obtained from an incompressible flow-over-a-square-cylinder experiment. The  $k - \epsilon$  parameters are estimated as a joint probability density function. Jet-in-crossflow simulations performed with  $(C_\mu, C_{\epsilon 2}, C_{\epsilon 1})$  samples drawn from this distribution are seen to provide far better predictions than those obtained with nominal parameter values. We also find a  $(C_\mu, C_{\epsilon 2}, C_{\epsilon 1})$  combination which provides less than 15% error in a number of performance metrics. In contrast, the errors obtained with nominal parameter values may exceed 60%.

## Nomenclature

$\mathbf{C}$	Turbulence model parameters; $\mathbf{C} = (C_\mu, C_{\epsilon 2}, C_{\epsilon 1})$
$C_\mu$	A parameter in the eddy-viscosity sub-model in a $k - \epsilon$ RANS model
$C_{\epsilon 2}, C_{\epsilon 1}$	Parameters in the equation of the evolution of $\epsilon$ in a $k - \epsilon$ RANS model
$\delta_m$	Structural error; difference between experimental data and calibrated surrogate model predictions
$\mathcal{N}(\mu, \sigma^2)$	Normal distribution with mean $\mu$ and standard deviation $\sigma$
$\mathcal{P}$	The set of probes being used for calibration
$y^{(p)}$	Reynolds stress predicted by RANS for probe $p$
$y_s^{(p)}$	Reynolds stress predicted by the surrogate model for probe $p$
$\mathbf{y}_e$	Experimental measurement of $\overline{u'v'}$
$d$	Approximation error in the surrogate model
AIC	Akaike Information Criterion
DES	Detached Eddy Simulation
IQR	Inter-quartile range
JIC	Jet-in-Crossflow
JPDF	Joint probability density function
LS	Learning Set
MAP	maximum <i>a posteriori</i> ; location of max. value of posterior probability density
MCMC	Markov chain Monte Carlo
TS	Testing Set

---

\*Technical Staff, Quantitative Modeling and Analysis, MS 9159

†Technical Staff, Quantitative Modeling and Analysis, MS 9152, Senior Member

‡Technical Staff, Aerosciences Department, MS 0825, Senior Member

## I. Introduction

Jet-in-crossflow (JIC) is a canonical flow problem of fuel-air mixing in scramjet engines.<sup>1</sup> It is also relevant in the flight dynamics of vehicles maneuvered by spin rockets, where the rockets' exhaust modifies the flow over control fins.<sup>2</sup> In most engineering settings, this interaction is simulated using Reynolds-Averaged Navier-Stokes (RANS) equations, in particular, with the  $k - \epsilon$  turbulence model. Prior investigations that compared a number of RANS formulations have shown that they are not very predictive for JIC studies.<sup>3</sup> Consequently, Large Eddy Simulations (LES) have been proposed as an alternative.<sup>4</sup> Others have postulated that the  $k - \epsilon$  model is fundamentally lacking and have attempted to estimate the  $k - \epsilon$  model deficiency by comparing against LES of JIC. The estimated uncertainty is thereafter propagated through to RANS predictions.<sup>1</sup> Both approaches have their drawbacks in a practical engineering situation. LES are extremely expensive and infeasible in routine engineering design where a huge number of runs have to be made. The second approach requires one to modify existing RANS codes, assuming one has access to the source code, and repeat the entire verification and validation exercise.

In this paper we will demonstrate an alternative approach to predictive JIC simulations, based on a *calibrated*  $k - \epsilon$  model. The  $k - \epsilon$  model<sup>5,6</sup> has four independent flow parameters and one that is kept at a constant ratio to one of the independent ones; if wall models are used, they may add a few more. The parameter values are considered to be *universal* and are evaluated by calibrating to Direct Numerical Simulations and experiments of simple flow configurations e.g., isotropic homogeneous turbulence, channel flow etc.<sup>6,7</sup> We call these parameter values the “nominal” ones. There is ample empirical evidence that these parameters are far from being universal<sup>6,8,9,10,11,12,13,14</sup> and the optimal parameter values can vary substantially from the nominal ones depending on the flow configuration. Thus there is no reason to suppose that the nominal values of  $k - \epsilon$  model parameters should yield accurate JIC simulations, and calibration, preferably to experimental data, should be a pre-requisite for their use in such settings. However, “wrapping” an optimizer e.g. L-BFGS<sup>15</sup> around a 3D JIC RANS simulation is hardly practical; the model is too computationally expensive for the O(100) sequential evaluations that might be required.

*We hypothesize that predictive JIC simulations can be obtained by calibrating a  $k - \epsilon$  model to a simpler but related flow problem.* The JIC flow is strongly vortical and in this paper, flow over a square cylinder<sup>16,17</sup> will serve as the calibration problem. The flow will be approximated using a 2D RANS  $k - \epsilon$  model, and  $(C_\mu, C_{\epsilon 2}, C_{\epsilon 1})$  will serve as the calibration parameters. Here,  $C_\mu$  is a parameter in the eddy-viscosity model while  $C_{\epsilon 2}, C_{\epsilon 1}$  appear in the evolution equation for  $\epsilon$ , the dissipation rate of turbulent kinetic energy.<sup>18</sup> We will first sample the  $(C_\mu, C_{\epsilon 2}, C_{\epsilon 1})$  space to seed 2D RANS simulations. The calibration observable  $(\overline{u'v'})$  will be recorded at each experimental probe location and their variation with  $(C_\mu, C_{\epsilon 2}, C_{\epsilon 1})$  will be represented using a surrogate model (a.k.a response surface model). We will investigate two surrogates: (1) based on polynomials and (2) a more complicated one, based on universal kriging. We will construct a separate surrogate for each probe. We will then pose a Bayesian inverse problem, predicated on the surrogates models, and conditioned on experimental data.<sup>16,17</sup> We will use an adaptive Markov chain Monte Carlo (MCMC) method to infer a joint distribution for  $(C_\mu, C_{\epsilon 2}, C_{\epsilon 1})$ . The calibration will be checked against the square cylinder measurements by performing a posterior predictive test i.e., we will attempt to reproduce the experimental results with the calibrated model. Thereafter, we will sample the joint  $(C_\mu, C_{\epsilon 2}, C_{\epsilon 1})$  distribution to seed an ensemble of 100 3D JIC simulations. The ensemble results will provide a probabilistic prediction of the flowfield and we will check its accuracy against available JIC experimental data.<sup>19,20</sup>

In Sec. II we review recent efforts to improve the predictive skill of RANS and LES JIC models. In Sec. III, we describe the construction and subsequent simplification of the polynomial models, the solution of the Bayesian inverse problem to estimate  $(C_\mu, C_{\epsilon 2}, C_{\epsilon 1})$  as well as a simple estimate of the model deficiency (or structural error) i.e., the inability of the *calibrated* RANS model to reproduce experimental data. These will be performed using the square-cylinder calibration test case. In Sec. IV we use the calibration (specifically the joint distribution of  $(C_\mu, C_{\epsilon 2}, C_{\epsilon 1})$ ) to estimate the improvement in JIC prediction accuracy, versus the nominal  $(C_\mu, C_{\epsilon 2}, C_{\epsilon 1})$  values, by comparing against JIC experiments. We conclude in Sec. VI.

## II. Background

The JIC interaction plays a central role in the control of finned bodies of revolution that are maneuvered by spin rockets; the exhaust from the rockets induce an angle of attack at the fins, significantly modifying the aerodynamic forces and moments.<sup>21</sup> The problem is strongly vortical and has been extensively studied

experimentally<sup>19,20,22</sup> (henceforth, collectively known as the “Beresh experiments”). The flowfield is dominated by a counter-rotating vortex pair, formed by a Kelvin-Helmholtz roll-up of the shear layer at the boundary between the jet and the crossflow. The vortex pair tracks the spatial evolution of the jet and has horse-shoe vortices wrapped around it. The counter-rotating vortex pairs and horse-shoe vortices are primarily responsible for the modification of the flowfield in the vicinity of the fins.<sup>2</sup>

Arunajatesan<sup>3</sup> performed a comparison of various  $k - \omega$  models<sup>18</sup> versus experimental JIC results. He found that all the  $k - \omega$  models over-predicted the turbulent intensities and Reynolds shear stresses inside the jet, resulting in a wider (“fatter”) jet vis-à-vis experiments i.e., the turbulent diffusion was over-predicted. However, the velocity field on a plane transverse to the streamwise flow (henceforth, the cross-plane) showed that the vortex pair resided at a point higher than the experimental measurements, a result at odds with the hypothesis of overly strong turbulent diffusion. He conjectured that turbulent stresses are underpredicted in the nearfield of the jet, resulting in an erroneous exchange of momentum between the jet and the crossflow. Investigations for various jet-to-crossflow momentum ratios and jet-crossflow cant angle revealed that the general behavior did not change, i.e., the lack of accuracy was characteristic of  $k - \omega$  models being investigated rather than the particular flow configuration.

The JIC problem has also been studied using LES<sup>23,24,25</sup> and Detached Eddy Simulations (DES<sup>26</sup>). The simulations were compared against the Beresh experiments, but only on the midplane (the plane of symmetry) and using mean velocities (streamwise and wall-normal) as the metrics of comparison. As expected, the comparison was far superior vis-à-vis RANS. The performance of these models in capturing the velocity/vorticity field on the cross-plane was not tested. While this is encouraging, LES and DES are too computationally expensive to be used in routine design calculations; however, they can serve as numerical experiments, which are then used to quantify the uncertainty in RANS models and to calibrate them.

Given the inaccuracy of RANS simulations (and not just in JIC interactions), it is natural to try and augment the empirical models for the creation and dissipation of turbulent kinetic energy with a “correction term”. The correction term is assumed to be spatially variable, is modeled statistically – usually as a Gaussian random field – and estimated from LES or Direct Numerical Simulations (DNS) data. This process is known as estimating the “structural” or “model-form” error in RANS models and has been performed for simple flows e.g., channel flow, flow over flat plate etc.<sup>27,28,29</sup> However, the method is very data-intensive i.e., in order to estimate the structural error, the “good” DNS/LES results have to be made available at each point of the RANS mesh. Edeling *et al.*<sup>30</sup> estimated, via MCMC, the structural error in  $k - \epsilon$  models using experimental boundary layer data under adverse and favorable pressure gradients. An alternative to calibration, which results in a more predictive RANS model, is to simply quantify the error/uncertainty in RANS predictions by comparing against LES data. This was outlined, for 2D flows, in Ref. 31, where turbulence variables from LES and RANS were compared to estimate the spatially variable difference/error. A statistical model (a probability density distribution) was created for the error. Thereafter, an ensemble of RANS simulations, each with a realization of the “error” field injected into it, were run to create an ensemble of predictions. Recently, this approach was extended to JIC computations.<sup>1</sup>

The studies described above assume that the nominal parameters of the RANS model are optimal and the deficiencies of RANS predictions require augmentation of the model. One could also postulate that the model should be *calibrated* first, i.e., estimate optimal parameters before embarking on a quest for structural errors. Such an approach, aimed at calibrating a LES model for JIC, is described in Ref. 4. The optimization of LES parameters, predicated on experimental data, was performed using surrogates of the LES model, constructed using kriging.<sup>32</sup>

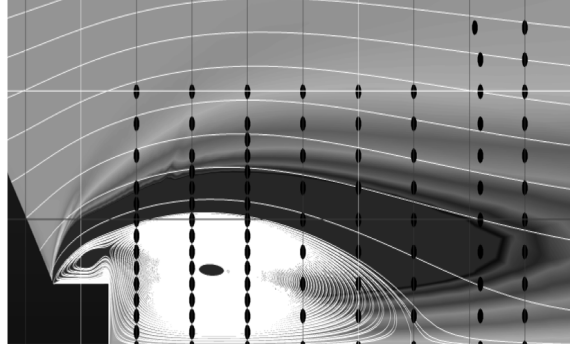
In this paper, we will describe a method to *calibrate* RANS models for JIC; the question of structural errors will be addressed in the future if the calibrated RANS model is found to be insufficiently accurate. Thus, conceptually, this work is similar to the LES calibration described in Ref. 4. However, we introduce two novelties:

1. Our calibration is Bayesian i.e., instead of obtaining a point estimate for  $(C_\mu, C_{\epsilon 2}, C_{\epsilon 1})$ , we construct a distribution for them. This distribution (henceforth, the “posterior distribution”) can then be used to perform an ensemble of JIC RANS runs to provide flow predictions as well as a quantification of prediction uncertainty.
2. We obtain our distribution of  $(C_\mu, C_{\epsilon 2}, C_{\epsilon 1})$  by calibrating to a strongly vortical, 2D flow over a square cylinder. 2D RANS simulations are computationally inexpensive (each run takes 4 minutes on 8 cores of a 2.6 GHz Intel Sandy Bridge processor), and our method for calibrating RANS models can be adopted in practical settings.

We demonstrate that the ensemble of predictions, obtained from the posterior distribution, results in far lower prediction errors (when compared against the Beresh experiments) vis-à-vis those obtained with nominal  $(C_\mu, C_{\epsilon 2}, C_{\epsilon 1})$  values (henceforth, “nominal predictions”). Further, the uncertainty bounds on the prediction are sufficiently tight such that some variables in the nominal predictions are relegated to being statistical outliers. Finally, we show that samples drawn from the posterior distribution can be used to identify predictive point estimates of  $(C_\mu, C_{\epsilon 2}, C_{\epsilon 1})$ , for use in JIC simulations.

### III. Calibration to a square-cylinder flow

In this section we describe the calibration of a 2D  $k-\epsilon$  model to experimental measurements of flow over a square cylinder. Per the discussion in Sec. I, there does not seem to be a universal value for  $(C_\mu, C_{\epsilon 2}, C_{\epsilon 1})$ ; consequently, we model them as random variables, whose joint probability density function (JPDF) is the object of calibration. The JPDF also allows us to accommodate uncertainty in the estimates due to limited experimental data. We expect that  $O(10^4)$  sequential evaluations of the  $k-\epsilon$  model will be required to obtain a converged  $(C_\mu, C_{\epsilon 2}, C_{\epsilon 1})$  JPDF. This is too computationally expensive even for 2D RANS and we will construct its surrogates, before posing and solving the Bayesian calibration problem.



#### III.A. Flow over a square cylinder

$(C_\mu, C_{\epsilon 2}, C_{\epsilon 1})$  are calibrated to measurements from a flow-over-a-square-cylinder experiment conducted in a closed water channel. Details of the experiment are in Refs. 16, 17 and we provide a summary below. The channel, with a 39 cm  $\times$  56 cm cross-section, is driven with a constant-head tank, with an average velocity of  $0.535 \text{ ms}^{-1}$ . The square cylinder, with dimensions of 56cm  $\times$  4cm  $\times$  4cm ( $W \times D \times D$ ) is mounted in the middle, resulting in a blockage ratio of 9.75%. The Reynolds number is 21,400 and the flow is statistically steady. Reynolds-averaged shear stresses  $(\overline{u'v'})$  and fluctuating velocities are measured in the upper half of the vertical mid-plane via laser Doppler velocimetry. Measurements are made at a set of “probe” locations arranged in a grid. The grid of probes begins at the leading edge of the cylinder, though for our paper we consider only those 96 probes which are in the wake. These are shown in Fig. 1 which also depicts the flowfield.

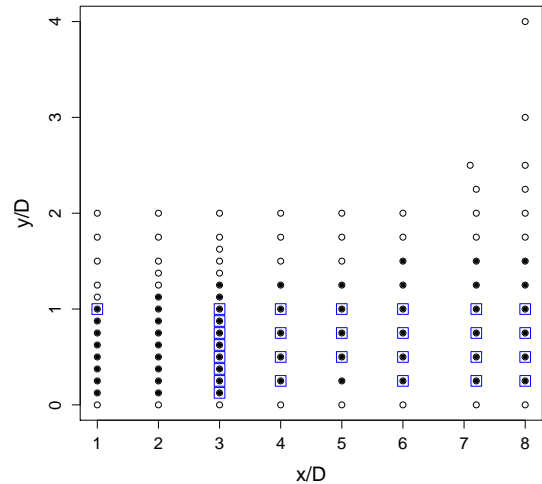


Figure 1. Above: Flood plot of the streamwise velocities with streamlines seeded just upstream of the cylinder and the location of the probes. The picture is not to scale. The dominant flow is left to right. Below: The location of all 96 probes (open symbols), the 55/96 for which surrogate models can be constructed with  $< 10\%$  error (filled symbols) and the 28/96 probes which are included in ProbeSet  $\mathcal{P}$  (in rectangles).

#### III.B. Construction of polynomial surrogates for 2D RANS

Let  $\overline{u'v'}$  at probe  $p$  be denoted by  $y^{(p)}$ . We postulate that the following cubic polynomial approximation holds:

$$\begin{aligned}
 y^{(p)} &= \sum_{l=0}^{l=3} \sum_{m=0}^{m=3} \sum_{n=0}^{n=3} \alpha_{l,m,n}^{(p)} (C_\mu)^l (C_{\epsilon 2})^m (C_{\epsilon 1})^n + d, \\
 &= y_s^{(p)} + d, \\
 3 &\geq l + m + n,
 \end{aligned} \tag{1}$$

where  $y_s^{(p)}$  is the polynomial approximation of  $y^{(p)}$  and  $d$  is the approximation error. In order to complete the model in Eq. 1, we first construct a dataset  $\{C_\mu, C_{\epsilon 2}, C_{\epsilon 1}, y^{(p)}\}$  to capture the variation of  $y^{(p)}$  with  $(C_\mu, C_{\epsilon 2}, C_{\epsilon 1})$ . We use space-filling Halton sequences<sup>33</sup> (as implemented in the `randtoolbox` package<sup>34</sup> in R<sup>35</sup>) to draw  $14^3$  samples from the  $(C_\mu, C_{\epsilon 2}, C_{\epsilon 1})$  parameter space and seed 2D RANS simulations of flow over a square cylinder. The number of samples to use was chosen as a compromise between the need to fully characterize the  $(C_\mu, C_{\epsilon 2}, C_{\epsilon 1})$  space and the number of 2D RANS simulations that could be completed in limited time. The values of  $y^{(p)}$  at the 96 probes are recorded, resulting in 96 separate  $\{C_\mu, C_{\epsilon 2}, C_{\epsilon 1}, y^{(p)}\}$  datasets for the probes. Eq. 1 is regressed to the datasets using least-squares minimization.

The cubic model so formed is rarely useful in practice due to its tendency to overfit the  $\{C_\mu, C_{\epsilon 2}, C_{\epsilon 1}, y^{(p)}\}$  data. We simplify the model by incrementally removing high-order terms and refitting the shrunk model to the same data. The (original) cubic model and its shrunk counterpart are competed using the Akaike Information Criterion (AIC); if the shrunk model results in a lower AIC, it is retained and subjected to the same incremental simplification process. We find that simplification removes terms from Eq. 1 for all 96 probes, and in some cases reduces the cubic model to quadratic.

We next test whether the AIC-based simplification procedure yields robust surrogate models. This is done via a 100-fold cross-validation test. The  $14^3$  RANS runs are separated into a ‘‘Learning Set’’ (LS) containing 2332 (approximately 85% of  $14^3$ ) randomly selected runs, while the remainder constitute the ‘‘Testing Set’’ (TS). The simplified polynomial model is fitted to the ‘‘Learning Set’’ and the relative error for each parameter combination  $i$  in the LS,  $\delta_{i,LS}^{(p)} = (y_i^{(p)} - y_{s,i}^{(p)})/y_i^{(p)}$ ,  $i \in \text{LS}$ , evaluated. The fitted model is also used to evaluate  $y_{s,j}^{(p)}$  for the parameter set  $j$  in the TS, and calculate the corresponding relative error i.e.,  $\delta_{j,TS}^{(p)} = (y_j^{(p)} - y_{s,j}^{(p)})/y_j^{(p)}$ ,  $j \in \text{TS}$ . These individual relative errors are summarized by their RMS (root mean square) value for the LS and TS. This process is repeated 100 times, using different LS/TS pairs; the mean of the RMS relative errors,  $\overline{\delta_{LS}^{(p)}}$  and  $\overline{\delta_{TS}^{(p)}}$ , are taken as measures of accuracy of the polynomial surrogate. The process is repeated for all the 96 probes.

In Fig. 2 we plot  $\overline{\delta_{LS}^{(p)}}$  and  $\overline{\delta_{TS}^{(p)}}$  for all the probes. We notice that the two relative errors have the same magnitudes i.e., the polynomial model fitted to the LS data is equally predictive of the TS. This indicates that the polynomial model does not overfit the LS data; had this not been the case,  $\overline{\delta_{LS}^{(p)}}$  would have been substantially smaller than  $\overline{\delta_{TS}^{(p)}}$ . We also notice that for certain probes the relative error is high i.e., the polynomial model is not an accurate representation of  $y^{(p)}$ , and should not be used in calibration. Using 10% error (green line in Fig. 2) as the criterion, we retain the 55 / 96 probes where the polynomial model is deemed to be sufficiently accurate.

### III.C. Bayesian calibration

The polynomial models for  $\overline{u'v'}$  at each probe  $p$  allow us to estimate  $\mathbf{C} = (C_\mu, C_{\epsilon 2}, C_{\epsilon 1})$  given experimental measurements  $y_e^{(p)}$ . Let  $\mathbf{y}_s = \{y_s^{(p)}\}$ ,  $p \in \mathcal{P}$ , be the predictions by the polynomial surrogates for a set of probes  $\mathcal{P}$ , corresponding to  $(C_\mu, C_{\epsilon 2}, C_{\epsilon 1})$ . Let  $\mathbf{y}_e = \{y_e^{(p)}\}$ ,  $p \in \mathcal{P}$  be the experimental values at the same set of probes. We model the experimental values at each probe  $p$  as

$$y_e^{(p)} = y_s^{(p)}(\mathbf{C}) + \delta_m, \quad \delta_m \sim \mathcal{N}(0, \sigma^2), \quad (2)$$

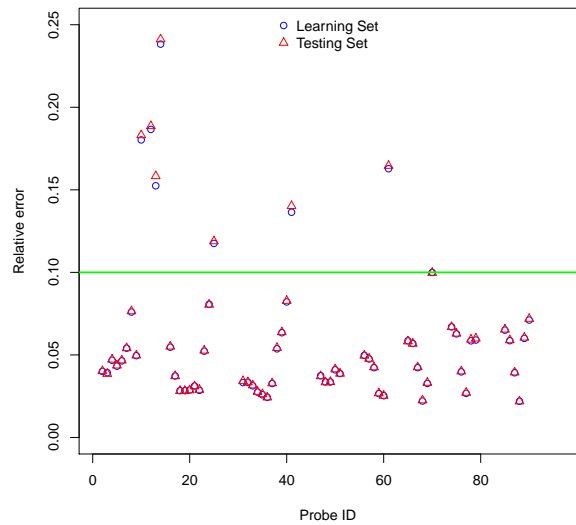


Figure 2. Comparison of  $\overline{\delta_{LS}^{(p)}}$  and  $\overline{\delta_{TS}^{(p)}}$  for all 96 probes. We note that the two relative errors are of the same magnitudes, indicating that there is little overfitting of the surrogates. We also see that for some probes, the relative errors can be big i.e., surrogates are not necessarily accurate for all probes. Some of the errors also lie outside the range of the vertical axis and are not plotted. The green line at 10% error demarcates the probes that can be used in calibration; the rest of the polynomial surrogates are too inaccurate for any practical use.

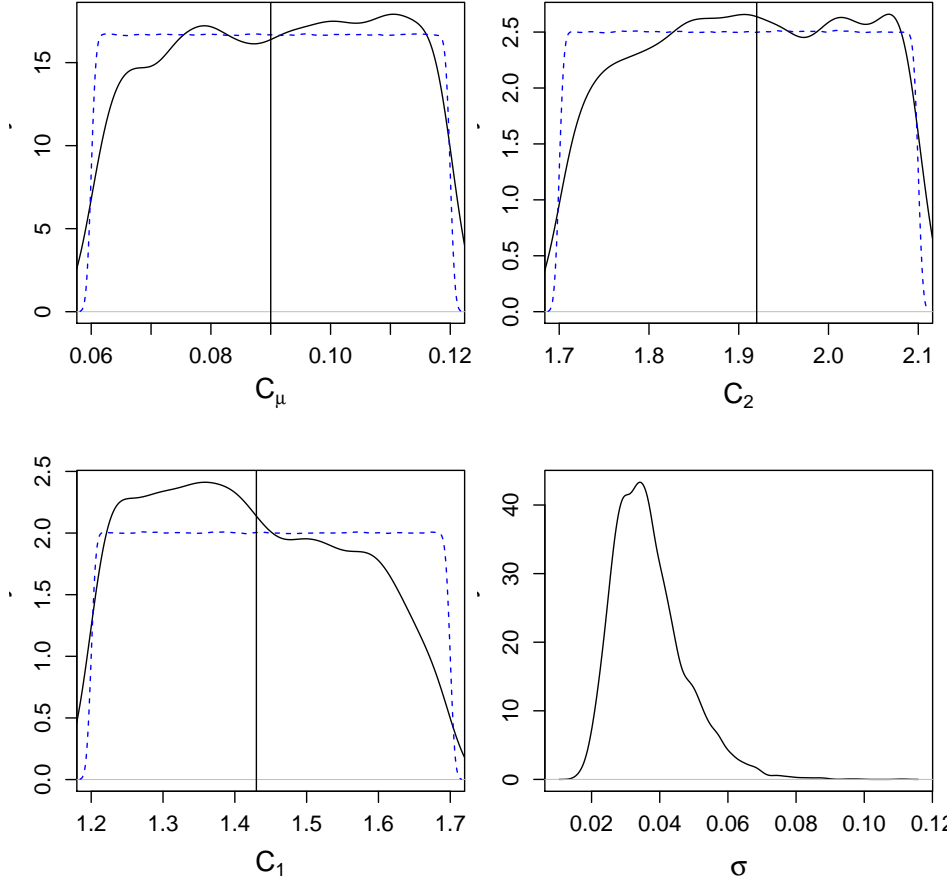


Figure 3. Plots of the posterior density for  $(C_\mu, C_{\epsilon_2}, C_{\epsilon_1})$ . The prior for each parameter is plotted with a dashed line. The vertical line denotes the nominal value. The rounded edge of the prior distribution is an artefact of the kernel-density estimation routine used for plotting.

where  $\delta_m$  is the model-data mismatch and  $\mathcal{N}(0, \sigma^2)$  denotes a normal distribution with zero mean and a standard deviation of  $\sigma$ . Then the probability  $P(\mathbf{y}_e|\mathbf{C})$  that the experimental data  $\mathbf{y}_e$  can be obtained using  $\mathbf{C}$  is

$$\begin{aligned}
 P(\mathbf{y}_e|\mathbf{C}) &= \prod_{p=1}^{|\mathcal{P}|} \frac{1}{\sqrt{2\pi}} \exp\left(-\frac{(y_e^{(p)} - y_s^{(p)}(\mathbf{C}))^2}{2\sigma^2}\right) \\
 &= \frac{1}{(2\pi)^{\frac{|\mathcal{P}|}{2}} \sigma^{2|\mathcal{P}|}} \exp\left(-\frac{\|\mathbf{y}_e - \mathbf{y}_s(\mathbf{C})\|_2^2}{2\sigma^2}\right)
 \end{aligned} \tag{3}$$

Here  $|\mathcal{P}|$  is the size of set  $\mathcal{P}$  i.e., the number of probes it contains. Let  $\pi_\mu(C_\mu), \pi_2(C_{\epsilon_2})$  and  $\pi_1(C_{\epsilon_1})$  be probability density functions (PDFs) reflecting our prior beliefs regarding the variation of turbulence model parameters. Then by Bayes' rule, the probability density (a.k.a the posterior density) of  $\mathbf{C}$  is

$$P(\mathbf{C}|\mathbf{y}_e) \propto P(\mathbf{y}_e|\mathbf{C})\pi_\mu(C_\mu), \pi_2(C_{\epsilon_2})\pi_1(C_{\epsilon_1}) \tag{4}$$

We construct a JPDF for  $\{C_\mu, C_{\epsilon_2}, C_{\epsilon_1}, \sigma\}$ , where  $\sigma$  serves as a nuisance variable and is marginalized over to obtain  $P(\mathbf{C}|\mathbf{y}_e)$ . The JPDF is constructed by sampling from the distribution (Eq. 3) using a Markov chain Monte Carlo (MCMC) technique.<sup>36</sup> Each sample requires one evaluation of the surrogate model for each probe in  $\mathcal{P}$  (defined below). For efficiency, we use an adaptive MCMC method called Delayed-Rejection Adaptive Metropolis,<sup>37</sup> as implemented in the R package FME.<sup>38</sup> About 25,000 samples are required to reach convergence, as measured by the Raftery-and-Lewis procedure,<sup>39</sup> implemented in `mcmcgsit`.<sup>40</sup> The prior

distributions used in this work are:

$$\begin{aligned}\pi_\mu(C_\mu) &= \mathcal{U}(0.06, 0.12), \\ \pi_2(C_{\epsilon 2}) &= \mathcal{U}(1.7, 2.1), \\ \pi_1(C_{\epsilon 1}) &= \mathcal{U}(1.2, 1.7),\end{aligned}\tag{5}$$

where  $\mathcal{U}(a, b)$  is the uniform distribution bounded by  $(a, b)$ .  $\sigma^{-2}$  uses a conjugate prior from the inverse gamma distribution; see Ref. 38 for details. The bounds for  $(C_\mu, C_{\epsilon 2}, C_{\epsilon 1})$  are taken from Ref. 6. The nominal values of  $(C_\mu, C_{\epsilon 2}, C_{\epsilon 1})$  are  $\mathbf{C}_{nom} = \{0.09, 1.92, 1.44\}$ .

Before we invert for  $P(\mathbf{y}_e|\mathbf{C})$ , we construct the ProbeSet  $\mathcal{P}$ . RANS predictions of  $\overline{u'v'}$  for  $\mathbf{C}_{nom}$  can have large errors vis-à-vis experiments, and we restrict  $\mathcal{P}$  to those probes where

$$\left| \frac{(y^{(p)} - y_s^{(p)}(\mathbf{C}_{nom}))}{y^{(p)}} \right| \leq 0.1 \quad \text{and} \quad \frac{1}{4} \leq \left| \frac{y_s^{(p)}}{y_e^{(p)}} \right| \leq 4.$$

Only 28 / 96 probes are included in  $\mathcal{P}$ ; these are plotted with squares in Fig. 1.

In Fig. 3 we plot the marginalized PDFs for  $C_\mu, C_{\epsilon 2}, C_{\epsilon 1}$  and  $\sigma$ . The nominal values are plotted as vertical lines. We see that the nominal values are contained in the support of the marginalized PDFs; further, there is no well-defined peak for  $(C_\mu, C_{\epsilon 2}, C_{\epsilon 1})$ . This implies a correlated JPDP for  $(C_\mu, C_{\epsilon 2}, C_{\epsilon 1})$ , potentially with multiple modes. Further, the PDF for  $C_\mu$  is not very different from the prior, indicating that  $\mathbf{y}_e$  is not very informative about it. The observations are somewhat more informative about  $C_{\epsilon 2}$  and  $C_{\epsilon 1}$ . The lack of a distinct mode also implies that estimating  $(C_\mu, C_{\epsilon 2}, C_{\epsilon 1})$  with a gradient-based optimization method could be difficult. In contrast, the PDF for  $\sigma$  has a well-defined peak, and consequently a maximum *a posteriori* (MAP, the location with the highest posterior probability density) value.

### III.D. Checking the calibration

We first conduct an interim check of the calibration by performing a posterior predictive test (PPT) i.e., we attempt to recreate the observations using the calibrated JPDP,  $\sigma$  and the polynomial surrogates. We draw 100 samples of  $\{C_\mu, C_{\epsilon 2}, C_{\epsilon 1}, \sigma\}$  from the JPDP, and use Eq. 1 to evaluate  $y_e^{(p)}$ , its median, the 25<sup>th</sup> and 75<sup>th</sup> percentiles. We plot these in Fig. 4 for the probes in  $\mathcal{P}$ , along with experimental values of  $\overline{u'v'}$  from Ref. 17 and predictions using  $\mathbf{C}_{nom}$ . We note that the inter-quartile range (IQR) spanned by the error bars capture the experimental measurements, whereas the medians are not particularly close to them - indeed, they are not very different from the nominal predictions. Thus by adopting a Bayesian approach to account for uncertainty caused by the model-data mismatch ( $\delta_m$ ) and limited experimental data, we have successfully constructed predictive, but computationally inexpensive, surrogate models.

Next, we verify the calibration using RANS simulations of flow over a square cylinder. This allows us to compare model predictions to experiments at locations where we do not have accurate surrogate models. As before, we use the 100 samples of  $(C_\mu, C_{\epsilon 2}, C_{\epsilon 1})$ . In Fig. 5 we compare  $\overline{u'v'}$  at the column of probes at  $x/D = 3$  and  $x/D = 8$ . RANS predictions are represented using the median and error bars corresponding to the IQR. Note that these predictions do not have  $\delta_m$  added to them. We also plot the velocity  $u$  at the two locations in the bottom of the figure. We see that the turbulent region inside the separation vortex is far smaller than the one observed in experiments. In Fig. 5 (left pair) we see that in computations, non-zero values of  $\overline{u'v'}$  are restricted to a small region. However post-calibration, the experimental values of peak

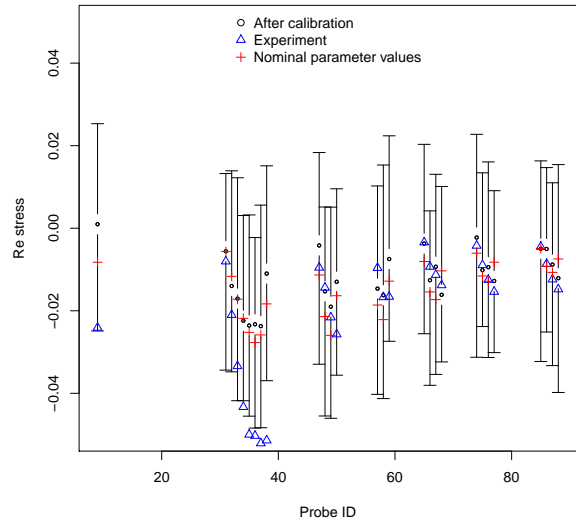


**Figure 4. Results from the posterior predictive test, performed with the polynomial surrogates. Results are only for probes in  $\mathcal{P}$ . The error bars denote the interquartile range (IQR) of the predicted  $\overline{u'v'}$ , while the circle is the median prediction. We see that most experimental readings lie in the IQR.**

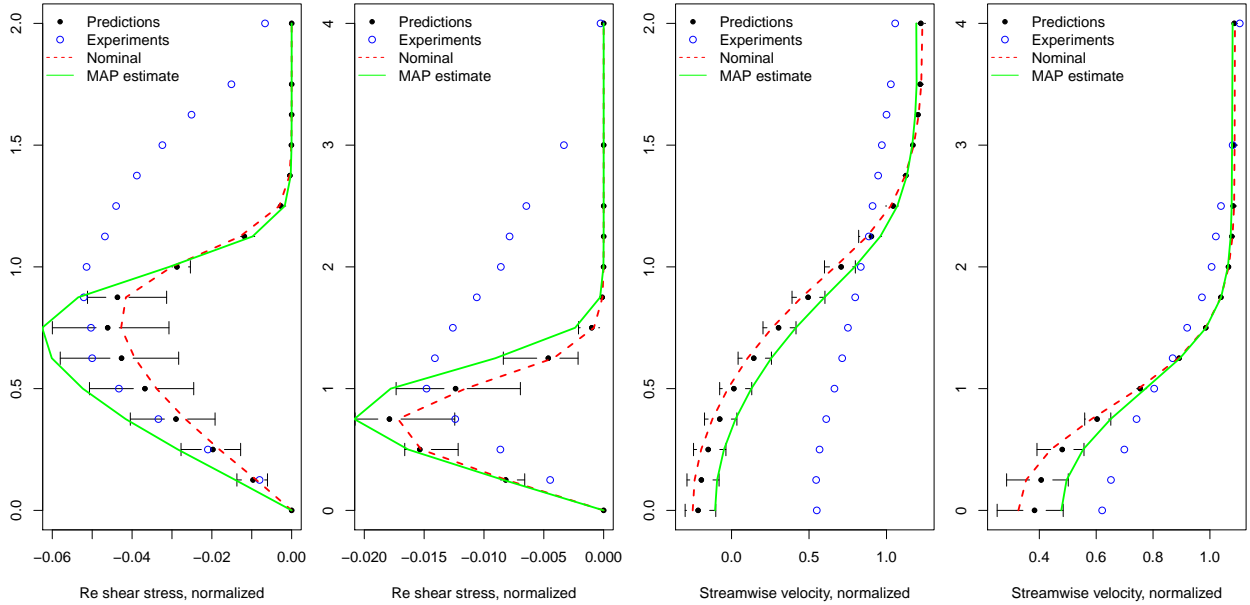


**Figure 5.** Comparison of predicted quantities from the 2D square-cylinder RANS simulations seeded using the calibrated JPDF. Left pair: Comparison of the experimental (symbols)  $\overline{u'v'}$  with the ensemble predictions (median and IQR) and predictions with  $C_{nom}$  (dashed, in red). The predictions using the MAP ( $C_\mu, C_{\epsilon 2}, C_{\epsilon 1}$ ) values are in green. Predictions are for columns of probes at  $x/D = 3$  and  $x/D = 8$  respectively. Right pair: Comparison of streamwise velocity  $u$  at the same locations.

Reynolds shear stress (defined as  $\overline{u'v'}$  for incompressible flow, as opposed to the more conventional  $\overline{\rho u'v'}$ ) are contained within the IQR of the numerical simulation results at  $x/D = 3.0$ . At  $x/D = 8.0$ , we see that the separation vortex experiences a smaller peak Reynolds stress in the experiment, as compared to numerical predictions. We note that the median predictions of  $\overline{u'v'}$  are not too different from those obtained by  $C_{nom}$ , and the net effect of Bayesian calibration is to add the credibility intervals. In Fig. 5 (right pair) we plot the streamwise velocity. We see clearly that the circulation in the vortex is over-predicted by the calibrated numerical simulation; the velocity is negative at  $y/D = 0$  and greater than  $U_\infty$  at  $y/D = 2$  at  $x/D = 3$ . In contrast, experimentally, the streamwise velocity is never negative and it reaches  $U_\infty$  at  $y/D = 2$ . At  $x/D = 8$ , the MAP estimates of  $(C_\mu, C_{\epsilon 2}, C_{\epsilon 1})$  predict a streamwise velocity which is very close to the experimental value (plotted in green).

## IV. Jet-in-crossflow predictions

We finally test the predictive skill of the calibrated JPDF on the JIC problem. The test case is described in detail in Refs. 3, 19, 20 and we produce a summary here. A supersonic jet exits from a nozzle into a  $12\text{in} \times 12\text{in}$  test section of a blow-down wind-tunnel. The tunnel Mach number is 0.8. The nozzle diameter,  $D_j$ , is 0.375in, has a design Mach number of 3.73 and is pointed vertically upwards. PIV (particle image velocimetry) measurements of velocities (mean and turbulent) are available along the spanwise symmetry plane and on a plane, perpendicular to the streamwise flow, at a location 33.8 jet diameters downstream (the cross-plane). The tunnel stagnation temperature is 320K and that of the jet is 300K. The ratio of the jet and freestream momentums is 10.2. In the RANS simulations, the inflow boundary is kept 10.66 jet diameters upstream. The coordinate system is anchored at the mid-point of the jet exit. The tunnel side and top walls are 16 and 32 jet diameters away. The top wall is modeled as a slip wall. The tunnel exit is 100 jet diameters downstream and characteristic non-reflective boundary conditions are imposed there. The entire jet nozzle, including the convergent part is meshed and included in the numerical model. The  $k - \epsilon$  RANS equations are solved using SIGMA CFD, an in-house research code in the Aerosciences Department at Sandia National Laboratories. The version of the model used corresponds to that in Ref. 41. Briefly, the high Reynolds number form of the  $k - \epsilon$  model is augmented with a modified version of the damping functions proposed in Ref. 42 for near-wall low Reynolds number regions. These equations are solved in a fully coupled form with the conservation equations for mass, momentum and energy using a conservative

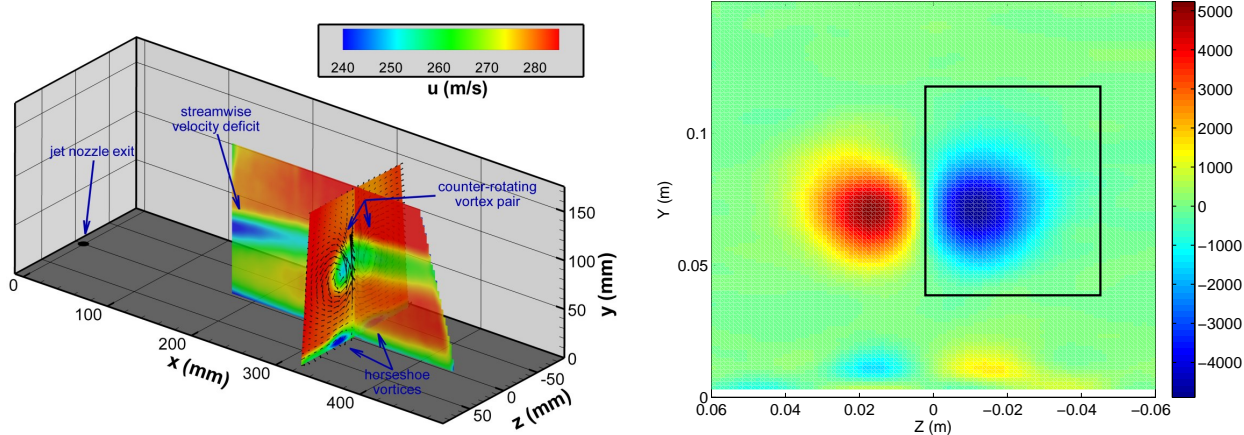


**Figure 6.** Left: A schematic of the simulation test case. Measurements are available at  $x/D_j = 33.6$  and  $z/D_j = 0$ . The figure shows the position of the jet and its roll-up into a counter-rotating vortex pair. Right: The streamwise vorticity field at  $x/D_j = 33.6$ . The box denotes the region of interest  $\mathcal{R}$  where we will quantify the vorticity as we test our calibration. Vorticity units in  $s^{-1}$ .

second order TVD finite-volume scheme in a block-structured solver. Fig. 6 shows the schematic of the test case, including the location of the jet, its roll-up into a vortex pair and the spanwise cross-plane at  $x = 33.6$  where the vorticity can be derived from experimental measurements. We define a rectangular region  $\mathcal{R}$ ,  $0.04m \leq y \leq 0.12m$ ,  $0 \leq z \leq 0.05m$  (the black box in Fig. 6 (right)), containing one of the vortices, where we will compute the metrics used to compare the calibrated versus nominal predictions.

We seed 100 3D RANS JIC simulations using  $(C_\mu, C_{\epsilon 2}, C_{\epsilon 1})$  samples drawn from the calibrated JPDF (the same samples used to make Fig. 3 and 5) and, for each simulation, quantify the vorticity in  $\mathcal{R}$  by calculating the circulation, the centroid  $(z, y)$  of the vorticity distribution and its radius of gyration (as an approximate measure of the vorticity distribution's spatial extent). These metrics are normalized by their counterparts calculated from experimental measurements.<sup>19,20</sup> In Fig. 7, we plot the RANS JIC predictions from the JPDF, and compare with those obtained using  $\mathbf{C}_{nom}$ . The box spans the IQR of the 100 predictions and the red line is the median. It is clear that the circulation is vastly overestimated before calibration; in fact, the calibrated predictions forming the IQR are all more accurate than the nominal predictions. However, the circulation is clearly overpredicted by the ensemble of numerical simulations. The centroid of the vorticity distribution also shows a bias:  $z$  is underpredicted whereas  $y$  is overpredicted. The nominal predictions fall within the IQR. The radius of gyration is also overpredicted, but the median prediction is almost perfect, and not very different from the nominal prediction. Thus the main improvement is in the circulation prediction.

The clustering of the IQRs around 1 raise the question whether there exists a  $(C_\mu, C_{\epsilon 2}, C_{\epsilon 1})$  combination for which the normalized predictions are all near 1. We define a goodness-of-fit score as the  $L_2$  norm of the relative errors in circulation, the centroid and the radius of gyration (calculated by subtracting 1 from the normalized values) and search the 100 samples for the one with the minimal score.  $\mathbf{C}_{opt} = \{0.117, 1.936, 1.262\}$  yields the smallest relative errors of 11.7%, -11.7%, -8.8% and 13.7% for circulation, the

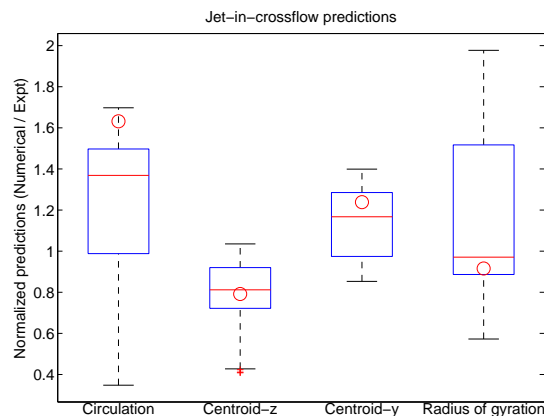


**Figure 7.** Distribution of normalized circulation, the location of the vorticity centroids and the radius of gyration, from JIC runs seeded by  $(C_\mu, C_{\epsilon 2}, C_{\epsilon 1})$  samples from the JPDF. The metrics calculated from a JIC simulation using  $\mathbf{C}_{nom}$  is plotted as a reference.

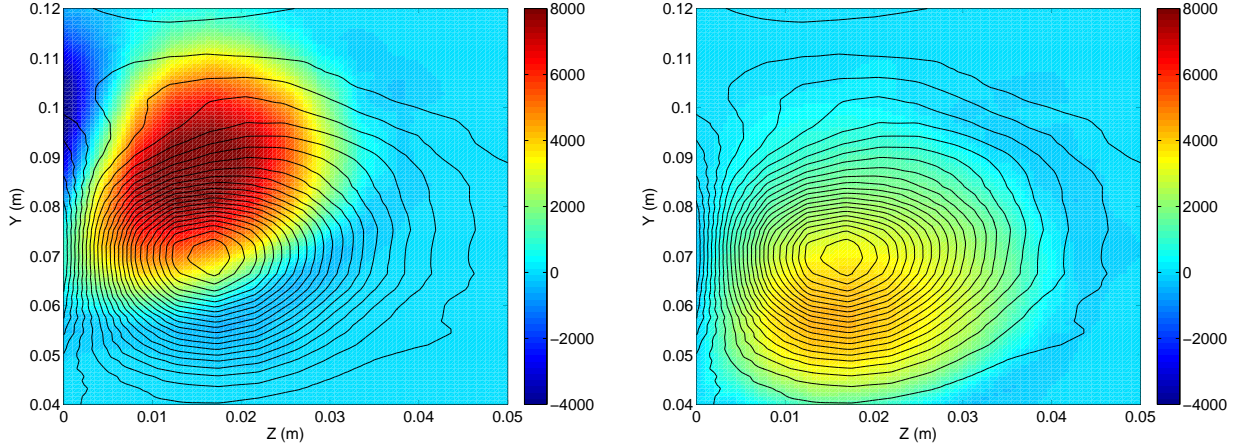


**Figure 8. Left: Vorticity predictions using  $C_{nom}$  with experimental results plotted as contours. Right: Predictions using  $C_{opt}$ . The improvement in the vorticity field is quite obvious - the uncalibrated vorticity prediction is too large and is in the wrong position. Vorticity is measured in  $s^{-1}$ .**

$z$ - and  $y$ -centroids and radius of gyration respectively. In Fig. 8 we plot the vorticity distribution predicted using  $C_{nom}$  (left) and  $C_{opt}$  (right). The experimental vorticity distribution is overlaid as contours. The improvement in the vorticity prediction is quite stark.

In Fig. 9 we check the ensemble prediction on the  $z = 0$  plane. We plot the streamwise velocity deficit  $(U_\infty - u(y))/U_\infty$  and vertical velocities  $v(y)$  at  $x/D_j = 31.5$  and  $42.0$ . We plot the experimental values (symbols), the ensemble predictions (median and IQR) and the solution corresponding to  $C_{opt}$  (green) and  $C_{nom}$  (red). We see that the velocity deficit is underpredicted by the ensemble as well as  $C_{opt}$ , but the vertical position of the peak deficit is approximately at the correct height. The improvements in the vertical velocity are more impressive. At both the locations, the vertical velocity predicted by  $C_{opt}$  is very close to the experimental results.

## V. Calibration with kriging surrogates

We perform calibration using not just a model for  $y_s^{(p)}$ , but also a Gaussian process model for  $d(C_\mu, C_{e2}, C_{e1})$  (see Eq. 1). A Gaussian process model (also called kriging) for  $d(C_\mu, C_{e2}, C_{e1})$  can be constructed provided its variation in  $(C_\mu, C_{e2}, C_{e1})$ -space is smooth. In its absence, i.e., if the variation of  $d$  resembles white-noise, the estimate for  $d$  will be near zero (the mean of white noise). The details of this method are given in Ref. 43. The rationale behind modeling  $d$  lies in providing a better approximation to  $y^{(p)}$  in Eq. 1. Since this is to be used in calibration, modeling  $d$  is relevant only if it is comparable (or larger) than the model-data mismatch  $\delta_m$  (Eq. 2); else, its effect can be subsumed into  $\delta_m$ . Fig. 3 shows that  $\sigma, \delta_m \sim \mathcal{N}(0, \sigma^2)$ , is large and it is unclear whether kriging  $d$  will make a difference.

In Fig. 10 we plot the distribution of  $C_\mu, C_{e2}$  and  $C_{e1}$  obtained by augmenting the polynomial models from Sec. III with a kriged model for  $d$ . Clearly, the results are unimproved. The evidence lies in the distribution for  $\sigma$ , which is virtually unchanged. Adding in the defect  $d$  made no impact on the model-data mismatch. Thus the more sophisticated surrogate is largely unjustified, even if one makes allowances for the time-consuming manual process of constructing them and the order-of-magnitude increase in computational times.

## VI. Conclusions

We have developed a method that could potentially be used for calibrating computationally expensive 3D RANS models. The method is based on Bayesian calibration to experimental data using surrogate models. The method was demonstrated by evaluating its impact on improving the predictive skill of RANS in JIC simulations. The adoption of a statistical calibration method allows us to accommodate the shortcomings of

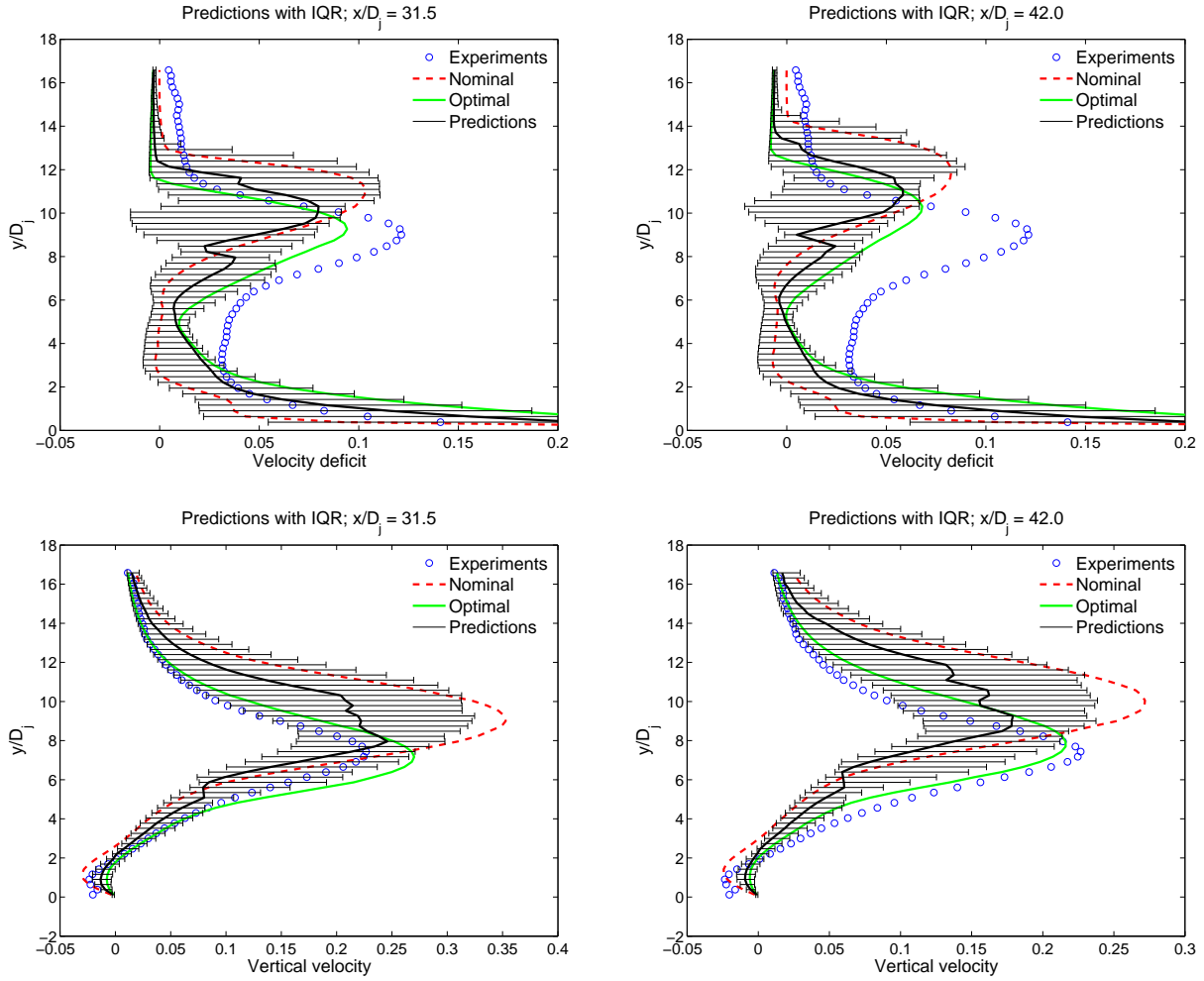


**Figure 9.** Above: We plot the streamwise velocity deficit  $(U_\infty - u(y))/U_\infty$  at  $x/D = 31.5$  and  $42.0$  on the  $z = 0$  plane of symmetry in the top two figures. We plot the experimental values (symbols), the ensemble predictions (median and IQR) and the predictions using  $C_{nom}$  (dashed, in red) and  $C_{opt}$  (green). Below: We plot  $v(y)$  at the same locations in the bottom two figures.

RANS in many flow configurations, as well as calibration issues due to limited experimental measurements.

In developing this method, we have introduced two new approaches. First, instead of calibrating a large problem as-is,<sup>4</sup> we search for a simpler, but related flow which can be simulated in an inexpensive manner. Since JIC is strongly vortical, we chose flow over a square cylinder as a calibration case. It can be simulated accurately under a 2D approximation, which simplified the calibration process.

Second, we introduce Bayesian calibration or parameter estimation. This method evaluates the model (2D RANS, in this case)  $O(10^4)$  times requiring us to create polynomial surrogates. We employed an existing model simplification method (using AIC) and demonstrated, via cross-validation, that the resulting models are robust i.e., they do not overfit. Further, Bayesian calibration allows us to predict in a probabilistic manner using an ensemble, rather than attempt to reproduce experimental data with a single set of model parameters. Thus we can account for the various approximations introduced during calibration.

Bayesian calibration using flow over a square cylinder yielded a JPDF that was surprisingly predictive for JIC. Its predictions were far more accurate than the nominal values of  $(C_\mu, C_{\epsilon 2}, C_{\epsilon 1})$ ; in fact, the quantification of uncertainty in predictions indicated that some nominal predictions were statistical outliers. Certain samples drawn from the JPDF yielded accuracies in vorticity generation which have never been achieved by RANS simulations of JIC.

We repeated our calibration using a surrogate that contained a kriging model for the defect  $d$  in Eq. 1. The model endows enhanced accuracy in  $y^{(p)}$  if  $d$  is smoothly distributed in  $(C_\mu, C_{\epsilon 2}, C_{\epsilon 1})$ -space. We find that this

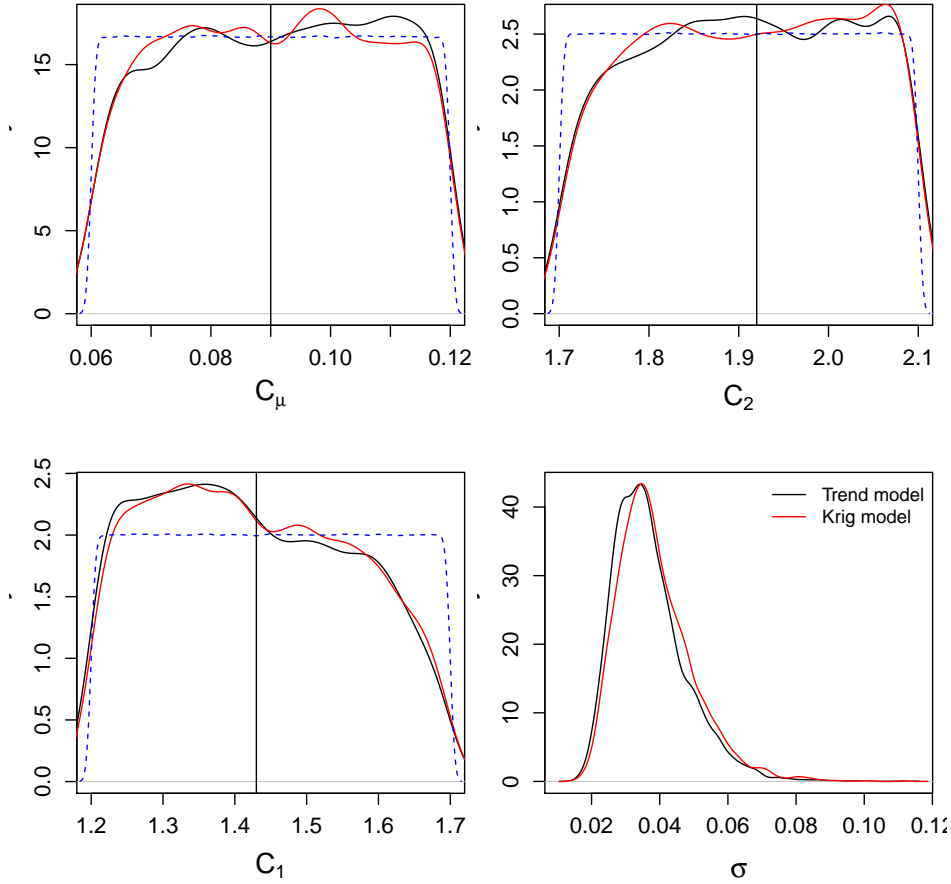


Figure 10. Marginal posterior distributions for  $C_\mu$ ,  $C_{\epsilon 2}$  and  $C_{\epsilon 1}$ , developed with surrogates with kriged  $d$ , are plotted in red. The black lines (“Trend model”) are densities obtained using a polynomial surrogate (Sec. III), whereas the dashed line is the prior.

enhanced accuracy does not lead to a calibration that is substantially different from the one obtained using  $y_s^{(p)}$ . The calibration, in this case, is determined by the ProbeSet  $\mathcal{P}$  and the difference between experimental observations and RANS predictions. Since the surrogates do not influence either of these issues, the same  $\mathcal{P}$  was used and the slight improvement obtained by modeling  $d$  paled into insignificance versus  $\delta_m$ , the measure of our inability, via RANS, to reproduce experimental observation. Since kriged models are significantly more complex than polynomial ones, we will de-emphasize their use in the future.

Finally, our method is conceptually and practically simple. The majority of the statistical methods used in this work are available as R packages; new development consisted mainly of postulating and testing various model forms (e.g., cubic in  $(C_\mu, C_{\epsilon 2}, C_{\epsilon 1})$ ). This is not difficult, and our method has the potential to be adopted in a practical engineering setting.

Our calibration efforts are still a work in progress. While we have developed the numerical tools to calibrate  $k - \epsilon$  models for JIC, we have only demonstrated them on a single test case. The predictive skill of the JPDF and  $\mathbf{C}_{opt}$  for other JIC configurations (Mach number, jet-freestream momentum ratios, and jet cant angles) has not been explored yet. However, the experimental data exists<sup>19,20,22</sup> and this investigation is underway.

To summarize, we have demonstrated that turbulence models can be calibrated in complex flow configurations. The calibration is Bayesian and yields turbulence model parameters as distributions. The calibration improves the accuracy of turbulent flow simulations. The statistical tools and software required to do so are freely available as R packages.

## Acknowledgment

This work was supported by Sandia National Laboratories' Advanced Scientific Computing (ASC) Verification and Validation program. Sandia National Laboratories is a multi-program laboratory managed and operated by Sandia Corporation, a wholly owned subsidiary of Lockheed Martin Corporation, for the U. S. Department of Energy's National Nuclear Security Administration under contract DE-AC04-94AL85000.

## References

- <sup>1</sup>Gorlé, C. and Iaccarino, G., "A framework for epistemic uncertainty quantification of turbulent scalar flux models for Reynolds-averaged Navier-Stokes simulations," *Physics of Fluids*, Vol. 25, 2013, pp. 055105.
- <sup>2</sup>Beresh, S. J., Heineck, J. T., Walker, S. M., Schairer, E. T., and Yaste, D. M., "Planar velocimetry of jet/fin interaction on a full-scale flight vehicle configuration," *AIAA Journal*, Vol. 45, No. 8, 2007, pp. 1827–1840.
- <sup>3</sup>Arunajatesan, S., "Evaluation of two-equation RANS models for simulation of jet-in-crossflow problems," *50th AIAA Aerospace Sciences Meeting*, 2012.
- <sup>4</sup>Jouhaud, J.-C., Sagaut, P., Enaux, B., and Laurenceau, J., "Sensitivity analysis and multiobjective optimization for LES numerical parameters," *Journal of Fluid Engineering*, Vol. 130, 2008, pp. 021401.
- <sup>5</sup>Jones, W. P. and Launder, B. E., "The prediction of laminarization with a two-equation model of turbulence," *International Journal of Heat and Mass Transfer*, Vol. 15, 1972, pp. 1–32.
- <sup>6</sup>Poroseva, S. and Iaccarino, G., "Simulating separated flows using the  $k - \epsilon$  model," Tech. rep., Center for Turbulence Research, Annual Research Briefs, 2001.
- <sup>7</sup>Kimura, I. and Hosoda, T., "A non-linear  $k - \epsilon$  model with realizability for prediction of flows around bluff bodies," *International Journal for Numerical Methods in Fluids*, Vol. 42, 2003, pp. 813–837.
- <sup>8</sup>Durbin, P. A., "Near-wall turbulence closure modelling without damping functions," *Theoretical and Computational Fluid Dynamics*, Vol. 3, 1991, pp. 1–11.
- <sup>9</sup>Durbin, P. A., "Separated flow computations using the  $k - \epsilon - v^2$  model," *AIAA Journal*, Vol. 33, 1995, pp. 659–664.
- <sup>10</sup>Yakhot, V. and Orszag, S., "Renormalization group analysis of turbulence," *Physical Review Letters*, Vol. 57, 1986, pp. 1722–1724.
- <sup>11</sup>Shih, T. H., Liou, W. W., Shabbir, A., and Yang, Z., "A new  $k - \epsilon$  eddy viscosity model for high Reynolds number turbulence flows," *Computers and Fluids*, Vol. 24, 1995, pp. 227–238.
- <sup>12</sup>Lumley, J. L., "Computational modeling of turbulent flows," *Advances in Applied Mechanics*, Vol. 18, 1978, pp. 123–177.
- <sup>13</sup>Ristorcelli, J. R., Lumley, J. L., and Abid, R., "A rapid-pressure covariance representation consistent with Taylor-Proudman theorem materially-frame-indifferent in the 2D limit," *Journal of Fluid Mechanics*, Vol. 292, 1995, pp. 111–152.
- <sup>14</sup>Grimaji, S. S., "Pressure-strain correlation modelling of complex turbulent flows," *Journal of Fluid Mechanics*, Vol. 422, 2000, pp. 91–123.
- <sup>15</sup>Byrd, R. H., Lu, P., Nocedal, J., and Zhu, C., "A limited memory algorithm for bound constrained optimization," *SIAM Journal on Scientific and Statistical Computing*, Vol. 16, No. 5, 1995, pp. 1190–1208.
- <sup>16</sup>Lyn, D. A. and Rodi, W., "The flapping shear layer formed by the flow separation from the forward corner of a square cylinder," *Journal of Fluid Mechanics*, Vol. 267, 1994.
- <sup>17</sup>Lyn, D. A., Einav, S., Rodi, W., and Park, J. H., "A laser Doppler velocimetry study of ensemble averaged characteristics of the turbulent near wake of a square cylinder," *Journal of Fluid Mechanics*, Vol. 304, 1995, pp. 285–319.
- <sup>18</sup>Wilcox, D. C., *Turbulence Modeling for CFD*, D C W Industries, 1998.
- <sup>19</sup>Beresh, S. J., Henfling, J. F., Erven, R. J., and Spillers, R. W., "Crossplane velocimetry of a transverse supersonic jet in a transonic crossflow," *AIAA Journal*, Vol. 44, No. 12, 2006, pp. 3051–3061.
- <sup>20</sup>Beresh, S. J., Henfling, J. F., Erven, R. J., and Spillers, R. W., "Penetration of a transverse supersonic jet into a subsonic compressible crossflow," *AIAA Journal*, Vol. 43, No. 2, 2005, pp. 379–389.
- <sup>21</sup>Peterson, C. W., Wolfe, W. P., and Payne, J. L., "Experiments and computations of roll torque induced by vortex-fin interaction," *42nd Aerospace Sciences Meeting and Exhibit, Reno, Nevada*, 2004.
- <sup>22</sup>Beresh, S. J., Heineck, J. T., Walker, S. M., Shairer, E. T., and Yaste, D. M., "Vortex structure produced by a laterally inclined supersonic jet in transonic crossflow," *Journal of Propulsion and Power*, Vol. 23, No. 2, 2007, pp. 353–363.
- <sup>23</sup>Chai, X. and Mahesh, K., "Simulations of high speed turbulent jets in crossflow," *49th AIAA Aerospace Sciences Meeting, Orlando Florida*, 2011.
- <sup>24</sup>Kawai, S. and Lele, S. K., "Dynamics and mixing of a sonic jet in a supersonic turbulent crossflow," *Center for Turbulence Research, Annual Research Briefs*, 2009.
- <sup>25</sup>Genin, F. and Menon, S., "Dynamics of sonic jet injection into supersonic crossflow," *Journal of Turbulence*, Vol. 11, 2010, pp. 1–13.
- <sup>26</sup>Rodebaugh, G. P., Brinckman, K. W., and Dash, S. M., "DDES of aeropropulsive flows based on an extended  $k - \epsilon$  RANS model," *51st AIAA Aerospace Sciences Meeting, Grapevine, Texas*, 2013.
- <sup>27</sup>Oliver, T. A. and Moser, R. D., "Bayesian uncertainty quantification applied to RANS turbulence models," *Journal of Physics: Conference Series*, Vol. 318, 2011, pp. 042032.
- <sup>28</sup>Cheung, S. H., Oliver, T. A., E. E. Prudencio, S. P., and Moser, R. D., "Bayesian uncertainty analysis with applications to turbulence modeling," *Reliability Engineering and System Safety*, Vol. 96, 2011, pp. 1137–1149.
- <sup>29</sup>Dow, E. and Wang, Q., "Quantification of structural uncertainties in the  $k - \omega$  turbulence model," *52nd AIAA/ASME/ASCE/AHS/ASC Structures, Structural Dynamics and Materials Conference*, 2011.

- <sup>30</sup>Edeling, W. N., Cinnella, P., Dwight, R. P., and Bijl, H., “Bayesian estimates of parameter variability in  $k-\epsilon$  turbulence model,” *Journal of Computational Physics*, Vol. 258, 2014, pp. 73–94.
- <sup>31</sup>Emory, M., Pecnik, R., and Iaccarino, G., “Modeling structural uncertainties in Reynolds-Averaged computations of shock/boundary layer interactions,” *49th AIAA Aerospace Sciences Meeting*, 2011.
- <sup>32</sup>Laurenceau, J. and Sagaut, P., “Building efficient response surfaces of aerodynamic functions with kriging and cokriging,” *AIAA Journal*, Vol. 46, No. 2, 2008, pp. 498–507.
- <sup>33</sup>Halton, J. H., “Algorithm 247: Radical-inverse quasi-random point sequence,” *Communications of the Association for Computing Machinery*, Vol. 7, No. 12, 1964, pp. 701–702.
- <sup>34</sup>Dutang, C. and Savicky, P., *randtoolbox: Generating and Testing Random Numbers*, 2013, R package version 1.13.
- <sup>35</sup>R Core Team, *R: A Language and Environment for Statistical Computing*, R Foundation for Statistical Computing, Vienna, Austria, 2012, ISBN 3-900051-07-0.
- <sup>36</sup>Gilks, W. R., Richardson, S., and Spiegelhalter, D. J., editors, *Markov Chain Monte Carlo in Practice*, Chapman & Hall, 1996.
- <sup>37</sup>Haario, H., Laine, M., Mira, A., and Saksman, E., “DRAM-Efficient adaptive MCMC,” *Statistics and Computing*, Vol. 16, No. 4, 2006, pp. 339–354.
- <sup>38</sup>Soetaert, K. and Petzoldt, T., “Inverse Modelling, Sensitivity and Monte Carlo Analysis in R Using Package FME,” *Journal of Statistical Software*, Vol. 33, No. 3, 2010, pp. 1–28.
- <sup>39</sup>Raftery, A. and Lewis, S. M., “Implementing MCMC,” *Markov Chain Monte Carlo in Practice*, edited by W. R. Gilks, S. Richardson, and D. J. Spiegelhalter, Chapman and Hall, 1996, pp. 115–130.
- <sup>40</sup>Warnes, G. R. and with contributions by Robert Burrows, *mcgibbsit: Warnes and Raftery’s MCGibbsit MCMC diagnostic*, 2011, R package version 1.0.8.
- <sup>41</sup>Brinkman K.W., Calhoon W.H., D. S., “Scalar Fluctuation Modeling for High-Speed Aeropulsive Flows,” *AIAA Journal*, Vol. 45, No. 5, 2007, pp. 1036–1046.
- <sup>42</sup>So R.M.C., Sarkar A., G. G. and J., Z., “A Dissipation Rate Equation for Low Reynolds Number and Near-Wall Turbulence,” *Theoretical and Computational Fluid Dynamics*, Vol. 9, 1997, pp. 47–63.
- <sup>43</sup>Lefantzi, S., Ray, J., Arunajatesan, S., and Dechant, L., “Tuning a  $k-\epsilon$  model for jet-in-crossflow simulations,” SAND Report SAND2013-8158, Sandia National Laboratories, Livermore, CA 94551-0969, September 2013, Unclassified and unlimited release.